ELSEVIER

Contents lists available at ScienceDirect

Journal of Nuclear Materials

journal homepage: www.elsevier.com/locate/jnucmat



Short communication

Unraveling the size fluctuation and shrinkage of nanovoids during *in situ* radiation of Cu by automatic pattern recognition and phase field simulation



M. Nasim^a, Sreekar Rayaprolu^b, T. Niu^b, C. Fan^c, Z. Shang^b, Jin Li^d, H. Wang^{b,e}, A. El-Azab^b, Y. Xue^{a,*}, X. Zhang^{b,*}

- ^a Department of Computer Science, Purdue University, West Lafayette, IN 47907, USA
- ^b School of Materials Engineering, Purdue University, West Lafayette, IN 47907, USA
- ^c The University of Hong Kong, Hong Kong Special Administrative Region
- d Institute of Special Environments Physical Sciences, Harbin Institute of Technology, Shenzhen 518055, Hong Kong Special Administrative Region
- ^e School of Electrical and Computer Engineering, West Lafayette, IN 47907, USA

ARTICLE INFO

Article history: Received 31 May 2022 Revised 4 December 2022 Accepted 5 December 2022 Available online 6 December 2022

Keywords: In situ radiation Nanovoids Void size fluctuation Phase-field simulation Machine learning

ABSTRACT

Void formation is an important aspect of irradiation response of metals. *In situ* transmission electron microscopy observation for void evolution during irradiation is an effective technique for studying void evolution. However, the amount of data collected during *in situ* studies drastically overwhelm the current capability for manual data analyses. Here, we used a data-driven approach where a convolutional neural network combined with greedy matching to detect and track nanovoid evolutions and migrations. This approach was able to discover the surprising phenomena of void size fluctuation and shrinkage during irradiation of Cu with pre-existing nanovoids. Phase–field simulations revealed the fundamental mechanism behind this *in situ* observed phenomenon of void size fluctuation.

© 2022 Elsevier B.V. All rights reserved.

Energetic particle irradiation introduces large numbers of point defects and their clusters such as dislocation loops and voids, into metallic materials [1-5], and leads to significant microstructure evolution [3,6-9]. Irradiation-induced voids and their evolution have motivated extensive research because voids lead to significant volume changes and degradation of mechanical properties [2,10–14]. In contrast to the universal observation of void growth under radiation, there are scattered studies showing void shrinkage during heavy-ion irradiation of metals, e.g., Ni or Cr ion irradiation induced void shrinkage in Ni [15,16]. Two concepts were proposed to explain this phenomenon. Steele and Porter suggested that injected self-interstitials led to the void shrinkage [15]. Dubinko et al. speculated that radiation-induced formation of highly localized and persistent anharmonic lattice excitations (called Quodons) interacted with voids and led to void shrinkage [17]. During the heavy-ion bombardment of metals, the displacement cascade events generate interstitials and vacancies [18]. The stochastic nature of these discrete cascade events at the atomistic scale, in turn, develops into fluctuations in point defect concentrations and fluxes [18–26]. These fluctuations play a significant role in the rate of secondary processes, such as dislocation climb and dislocation loop growth [18,20]. Also, fluctuations in point defect fluxes are shown to affect the kinetics of void-size distribution resulting in the drift of voids along the size spectrum [21–26]. Consequently, one would anticipate that void size may also fluctuate during irradiation due to the fluctuations in point defect fluxes. However, such void size fluctuation phenomenon was rarely reported through experiments.

In situ radiation experiment inside a transmission electron microscope provides an important way to analyze the radiation induced void evolution [27–29]. Nevertheless, the analysis of in situ video data containing tens of thousands of micrographs demands a significant devotion of time and manpower and thus necessitates the development of automatic image/video analysis tool. Here we propose an Artificial Intelligence enabled automated measurement system capable of detecting and tracking voids at nanometer scale and demonstrate its application on the novel scientific discovery of void size fluctuations.

The task of identifying defects in videos resembles image segmentation under human supervision. Recently, a convolutional neural network (CNN) based approach has been proposed for defect identification in materials [30], where a convolutional neural network trained with a few image samples labeled manually, is

^{*} Corresponding authors.

E-mail addresses: yexiang@purdue.edu (Y. Xue), xzhang98@purdue.edu
(Y. Zhang)

used for identifying defects. A key limitation of this approach is the huge manual effort required to obtain labeled samples. An image with resolution 1000×1000 , contains a million pixels. To use this image as a training sample for CNN, each pixel must be labeled manually first. Because of this daunting requirement, only 2 images were labeled in a previous study [31]. An efficient approach to obtain labeled data is essential to make the neural network model robust against drift and contrast variance during radiation experiments.

In this study, a greedy tracking algorithm was introduced to associate CNN detections and track nanovoids during radiation. Using the machine learning based automatic tools, we discovered void size fluctuations during the in situ radiation of Cu, which were previously unnoticed. The machine learning tool also permits us to reliably describe size-dependent void shrinkage and determine the diffusivity of nanovoids during radiation. Phasefield simulation was performed to unveil the physics behind the radiation induced void size fluctuation. Over the years, a great deal of simulation efforts has been devoted to understanding the displacement cascade structure and evolution; however, it is hard to justify the modeling results from experiments due to the spatial and temporal resolution limitation. The fluctuation of the void sizes based on our tracking results provides important experimental evidence of the proposed displacement cascade structures. This study provides one of the first examples that combines artificial intelligence, machine learning, in situ radiation and phase-field simulation to study irradiation induced void evolution.

The data used for our study of void evolutions was obtained from *in situ* radiation experiment on sputtered single-crystal Cu (110) films. Plan-view transmission electron microscopy samples were mechanically grinded and polished, followed by dimpling and low energy Ar ion milling by using a Gatan PIPS II system. The TEM foil thickness was measured to be 115 nm based on the convergent beam electron diffraction (CBED) measurements. The *in situ* radiation experiment was conducted in the Intermediate Voltage Electron Microscope (IVEM) at Argonne National Laboratory, operated at 350 °C, where an ion accelerator is attached to a Hitachi-900 TEM. All the TEM specimens were annealed for 0.5 h at 350 °C, prior to the 1 MeV Kr⁺⁺ irradiation up to a fluence of 2×10^{14} ions/cm². The maximum dose was 1.0 dpa, at a dose rate of 3×10^{-4} dpa/s.

To analyze the video data obtained during the *in situ* radiation experiment, detect-and-track system using a combination of U-Net (a convolutional neural network) and a greedy matching algorithm was developed. U-Net is a fully convolutional neural network with skip connections, which was first used for biomedical image segmentation [31]. To obtain the labeled data for training U-Net model, a specially designed labeling tool was developed, which first takes a video frame as input and breaks it into multiple segmented superpixels based on color and spatial proximity. These superpixels are formed using Simple Linear Iterative Clustering algorithm (SLIC) [52]. With this interactive tool, voids in a frame can be labeled in a few minutes. Out of 7455 total frames, we labeled 75 frames with this labeling tool. With these labeled images, we trained the U-Net model for 500 iterations. The labeled images were downsized to a resolution of 256×256 pixels. For optimizing the neural network, we used binary cross entropy loss, where a value of 1 indicates that a pixel belongs to a void, while a 0 value denotes that it does not belong to any void. For training, a batch size of 20 and a learning rate of 0.01 was used. Finally, the trained network was applied on all 7455 frames of the video to identify voids present in each frame.

To investigate the reason behind void size fluctuation, we performed phase-field simulations of void evolution. The void defect evolution is characterized by concentration variables governed by Cahn-Hilliard type equations and the phase-field variable, which

identifies the phase at any given point in the domain, governed by the Allen-Cahn equation. Different models have been proposed to capture the kinetics [32–43], but we choose the model developed and reported in [44-46]. We solve the non-dimensionalized equations of the model and include the effects of temperature qualitatively through the ratio of vacancy to interstitial diffusivities D_{ν}/D_{i} . To model the kinetics at an elevated temperature, we set the latter ratio to be equal to 0.2. The physical size and distribution of vacancies and interstitials resulting from the displacement cascade event are modeled by considering a core-shell structure in the cascade zone. Vacancies occupy the core of the damage and interstitials at the periphery surrounding vacancies. However, we note that to accurately model the distribution of point defects in the cascade zone, a coupling between the models that captures the physics at the lower scales-length and time-and the mesoscale phase-field simulations is necessary [47]. Nonetheless, the simple core-shell structure is sufficient to explain the void-size fluctuations observed in the experiments. The simulation domain has a total of 151×101 grid points with the solid region occupying 101×101 grid points, and the rest is an empty space. More details on the phase-field model could be found in the supplementary information.

An example of the defects identified by the trained U-Net model is shown in Fig. 1. We evaluated the performance of our trained U-Net model on a test set of 30 labeled images. The performance metrics are accuracy and the pairwise intersection-over-union (IOU) score, which measures the ratio of the intersection over the union of the ground-truth nanovoid region to that predicted by the U-Net model. We found that our trained model had on average, a pixelwise accuracy of 99.78% and an IOU score of 86.00%. For the training set used to originally train the U-Net model, both the accuracy and the IOU score were 100%.

To track the positions and sizes of nanovoids in the entire video, a greedy matching algorithm was developed based on overlaps between detected nanovoids in consecutive frames. We first define a potential movement region for each detected void in each frame. Then for a pair of consecutive frames, we calculate the overlap between the potential movement regions. We then match the voids greedily based this overlap, prioritizing higher overlapping scores. Details of the tracking algorithm is presented in the supplementary materials.

The combination of U–Net and greedy matching produces a set of superpixels for each frame, where each superpixel denotes a void shaped defect. To calculate the sizes of these voids, we first find the centroid of these superpixels and compute the distance of the boundary pixels from the centroid. The median of these distances is then doubled to obtain the diameter of each void. Fig. 2a shows the sizes of several different voids, measured with the process described above. To account for the noise in the video and the U–Net model, a rolling average of 15 measurements was used to plot each point and the total number of analyzed frames is 5430. Comparisons between actual measurements from U–Net mode, average measurements and manual measurements are shown in Fig. 2c and d.

As shown in Fig. 2a, the sizes of the voids do not change monotonically, instead, they fluctuate constantly. To quantify the degree of fluctuation, we define size fluctuation of the voids as the difference between consecutive local maxima and local minima for the plot shown in Fig. 2a. Fig. 2b shows the gaussian kernel density function estimated from these fluctuation measurements. In Fig. 2b, six voids of different initial sizes were selected and compared to emphasize the difference in their degree of fluctuations. We see here that the larger voids have a narrow peak around 0. The voids with a smaller initial size have a lower peak value and wider distribution profile compared to the larger voids. This difference implies that larger voids undergo small changes in size, while smaller voids undergo comparatively greater size fluctuations. To

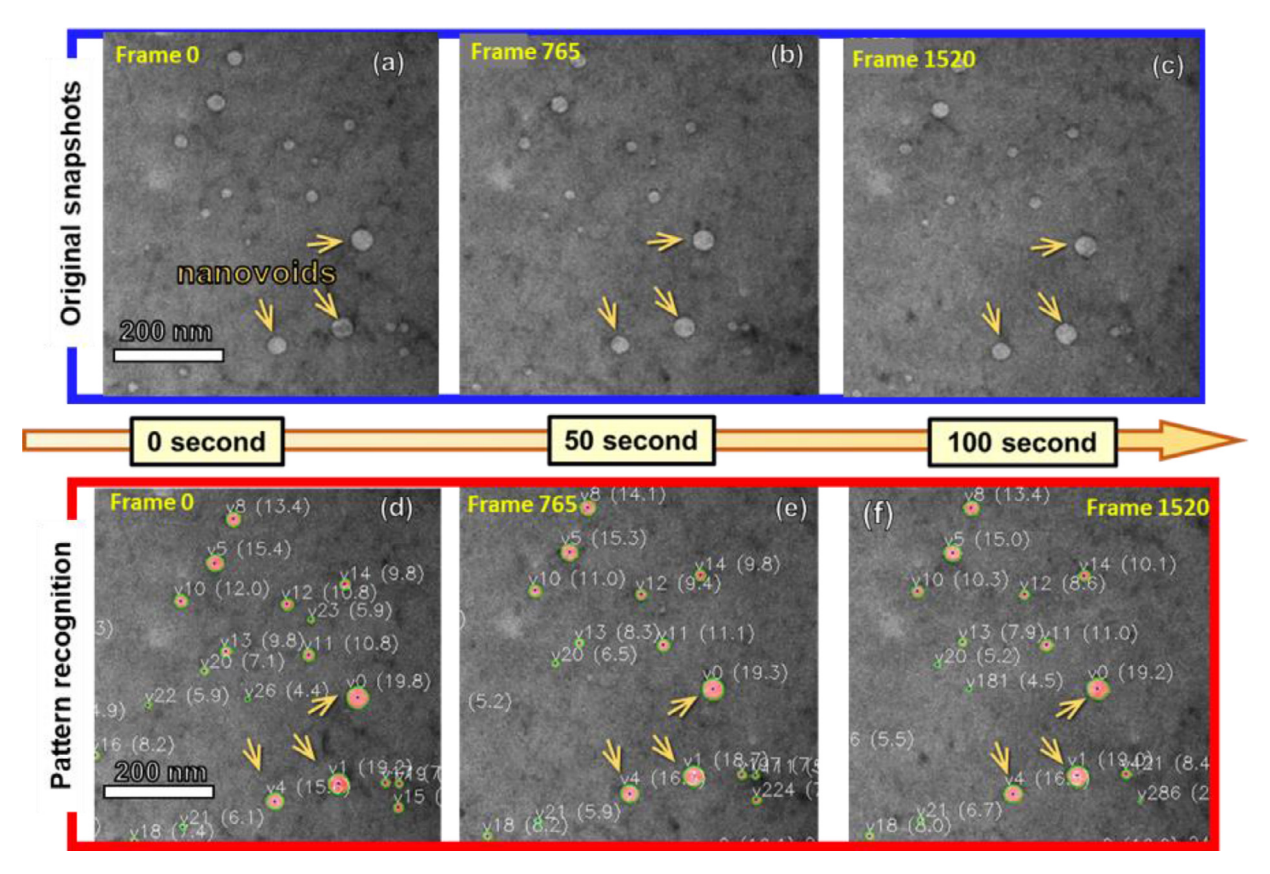


Fig. 1. Pattern recognition of TEM micrographs of nanovoids in Cu (110) film captured during in situ Kr ion irradiation at 350 °C, over 0.5-0.6 dpa. (a-c) In situ TEM radiation snapshots taken at 0, 50, and 100 s, respectively. (d-e) The nanovoids present in the corresponding snapshots as detected by the U-Net model (Numbers in bracket represent the diameter of nanovoids in unit of nm).

confirm the void size fluctuation, manual measurements were performed for selected nanovoids. As shown in Fig. 2c-d, voids of different initial size show various magnitude of fluctuation as confirmed by in-depth TEM analyses. To confirm that the void size fluctuation is a real phenomenon, and not a result of error arising from rastering of ion beam, we compared the results from two in situ radiation experiments, with and without beam rastering. We found that irrespective of the presence of beam rastering, void size fluctuation was observed frequently as shown in Fig. 3. The manual measurement, along with the experiments with and without beam rastering confirms that void size fluctuation indeed is a physical phenomenon, hence providing one of the first empirical evidence for the random size fluctuation. In addition to the void size fluctuations over short period of time, the long-term (over 3 min) size variations of the voids in Fig. 4a shows the voids undergo shrinkage in different magnitudes. The voids with smaller initial size shrink more compared to the larger voids, in agreement with the previous studies of void size evolutions [27–29].

Void swelling, accompanied by significant volumetric expansion, is often observed in metallic materials subjected to radiation damage. In contrast to conventional anticipation, the nanovoids in Cu (110) film were found to shrink constantly under high temperature *in situ* radiation. The shrinkage of porosity has been previously reported in nanoporous (NP) Ag, NP Au and single crystal–like Cu embedded with nanovoids under room temperature radiation [29,48,49]. Such void shrinkage phenomenon is tightly associated with the preferential absorption of interstitial type of defects by void surfaces. The stress field analysis suggested the existence of strong tensile stresses in the vicinity of voids, resulting in reduced loop migration energy, thereby facilitating the absorption of interstitial loops by void surface

[27]. Recent phase–field simulation study also reveals that the biased interstitial flux to void would lead to the shrinkage of voids and the void shrinkage rate was inversely proportional to the original void diameter [29]. The larger curvature of smaller voids may foster a higher concentration of interstitials and accelerated interstitial diffusion, leading to the faster shrinkage of smaller voids.

The key bottleneck that prevented the discovery of void size fluctuations previously is the simultaneous need for in situ TEM radiation of specimens with voids and the insurmountable effort required to manually analyze the hundreds of thousands of TEM micrographs with high precision. Most prior manual analyses used sampling techniques to examine only a small fraction of discrete frames, where noticeable changes can be identified with naked eyes. However, as void size fluctuations occur rapidly and the dimension of variation is often at small scale, it is not readily apparent from visual inspection or partial sampling of TEM data. The lack of automated high-fidelity TEM micrograph analyses prevented the discovery of void size fluctuation phenomena. Our machine learning based detect-and-track system can overcome this limitation by automating the manual analysis process. By using only a few TEM micrographs, labeled with human supervision, our machine learning model can detect nanovoids in thousands of frames with high precision. The greedy matching is then able to associate the voids in different frames, enabling us to track the changes in these voids (size, geometry, position, migration etc.). To confirm the detection of void size fluctuation obtained from our model, we performed manual TEM analyses (Fig. 2c-d) and found the results to be highly accurate (99% pixelwise accuracy).

Prior studies also suggest that nanovoids could become mobile during irradiation at elevated temperatures. *In situ* TEM experi-

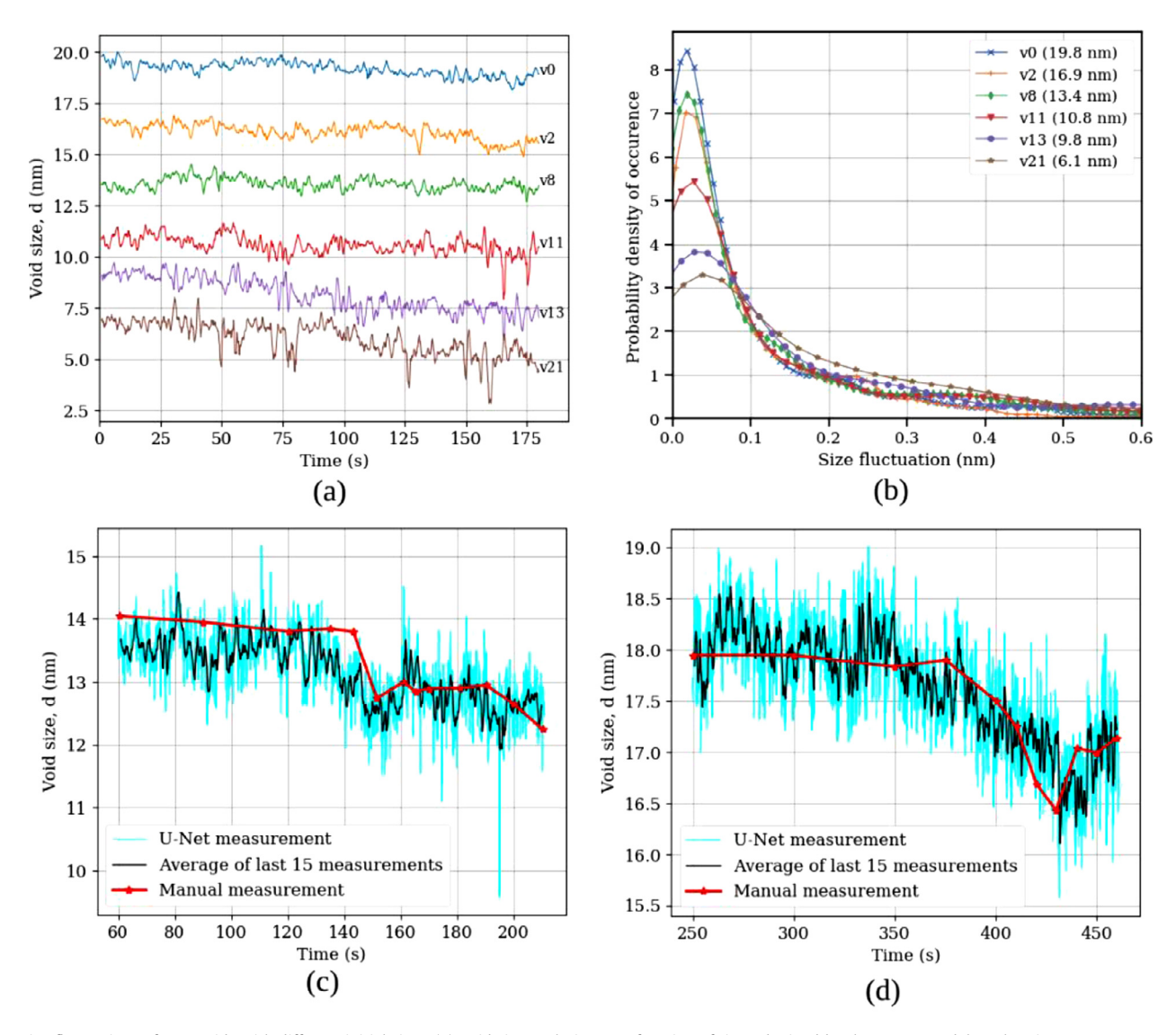


Fig. 2. Size fluctuations of nanovoids with different initial sizes. (a) Void size evolution as a function of time obtained by the U-Net model. Each point represents an average over 15 measurements. (b) The estimated density distribution (Gaussian kernel) of size fluctuation of various nanovoids. (c-d) Fluctuations were measured as differences between consecutive local maxima and local minima. Comparison between size obtained from U-Net model output (actual and average) and manual measurement (discrete data-lines) of a nanovoid with initial size of (c) 14.0 nm and (d) 18.0 nm. The manual analysis (obtained from examination of TEM snap shots) is in agreement with model calculations.

ments have been performed to trace the migration of voids and defect clusters (such as dislocation loops) [48,50]. In Fig. 4c, we show the mean square displacement of 9 voids detected as measured by the U–Net model, while in the Fig. 4b we show the mean square displacement of the average void size—computed for the void sizes in the range 9–18 nm. The mean square displacement is related to the diffusion behavior of the voids. Void motion imitates a random walk under cascade condition, and one should be able to extract the individual diffusivities of the voids, in addition to an effective diffusivity. The time dependent mean-square-displacement of voids is plotted (see supplementary Fig. S4). The diffusivity of nanovoids (D) can be calculated as:

$$\overline{r^2} = 6Dt \tag{1}$$

where $\overline{r^2}$ is the mean square displacement and t is time. The individual diffusivities for the 9 voids of varying sizes were found to be in the range 0.106-0.270 nm²/s, while the diffusivity of the average-sized void turned out to be 0.167 nm²/s. In Fig. 4d, we plotted the individual diffusivities of the 9 voids against their initial sizes, where the diffusivities of the voids decrease

exponentially with an increase in the void size, in agreement with an earlier study [50]. The mean square displacement of the larger voids seem to be varying linearly with time, while the smaller voids, upon close observation, deviate from the linearity (see supplementary Fig. S5). This size-dependence of the mean square displacement against time could be explained based on the amount of void diameter reduction reported in Fig. 4a. The smaller voids shrink more than the larger voids in the time interval for which the void evolution was analyzed using the U-Net model. Therefore, the larger voids migrate with their size remaining almost the same throughout the time interval, whereas the smaller voids shrink significantly, thus explaining their deviation from the linear behavior. The size-dependence of the void diffusivity could be explained based on the atom transport mechanism. There are various atom transport mechanism in metals. For example, surface diffusion of atoms, volume diffusion of atoms and, finally, the vapor transport of matter between the boundaries of the cavity. Of all the three different atom transport mechanisms, the velocity of the void decrease with an increase in the void size only for the atom transport through surface diffusion [51], thus

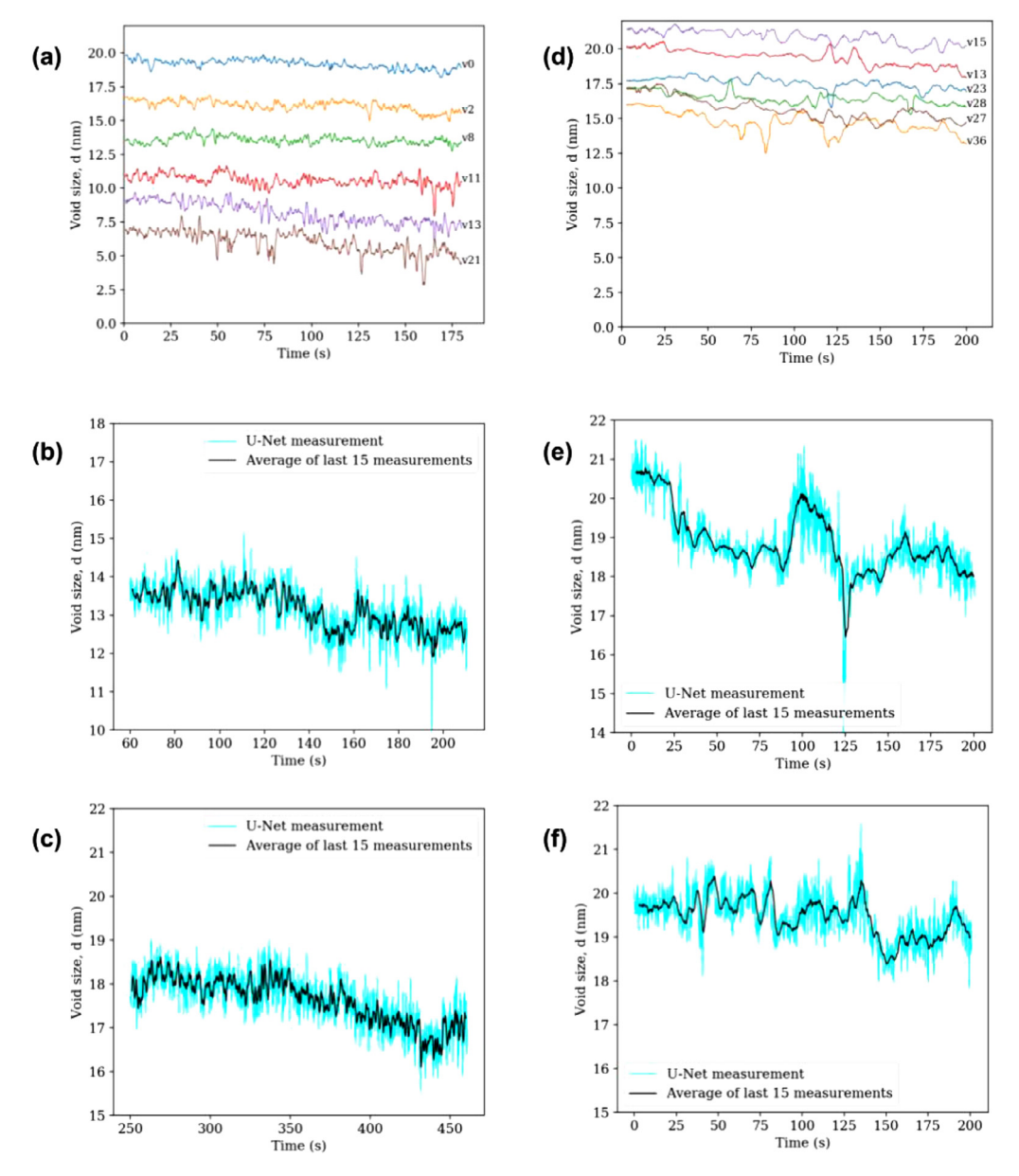


Fig. 3. Void size fluctuations for different sized voids during in situ irradiation of NV Cu (110), with beam rastering (a-c), and without beam rastering (d-f). Void size fluctuations appear as random processes in both cases. For different size of the voids, the magnitude of fluctuations also varies.

explaining the apparent size-dependence void diffusivity in our observations.

Previously, defect migration and diffusivity study have been conducted for Ag [49,51], Au [48] with in situ experiment. The diffusivity of defect clusters (likely to be a mixture of vacancy and interstitial clusters) in nanoporous Au during in situ Kr radiation at room temperature is $4\pm 2~\text{nm}^2/\text{s}$ [48]. The much smaller diffusivity of voids compared to defect clusters may indicate the higher energy barrier to activate void migration. Our study is the first one to compute void diffusivity in Cu, and we performed this analysis on a much finer scale (9 voids of initial size 9-18 nm diameter, and 2700 readings for each void was used to compute the mean square displacement as shown in Fig. 4b). We show this mean square displacement, calculated using the data obtained from our machine learning model, as a proof that our model is not limited to size measurement only and can be generalized to analyze other material properties of interest. Our study is a concrete example, proving that the integration of AI can greatly accelerate scientific discoveries and help uncover new materials physics.

To probe the physics of size-dependency of void size fluctuations, we performed two phase-field simulations, one with a void of radius six pixels and another with a void of radius twelve pixels. In each case, the void is initialized at the center of the domain. The cascades hit locations near the void, five grid points away from the surface on four sides of the void (Fig. 5a). As a result, the fluctuations will be of significant magnitude and aid in identifying the differences in amplitudes of fluctuations between voids with different sizes. The initial concentration of point defects in the matrix is set to thermal equilibrium values. The cascades are biased towards releasing a higher number of interstitials than vacancies to account for the observed formation of stacking-fault tetrahedrons during irradiation (see supplementary Fig. S3). For example, for every 100 interstitials introduced into the periphery of the core-shell structure. 90 vacancies are created within the core. We also note that void size fluctuations will be maximum when equal amounts of in-

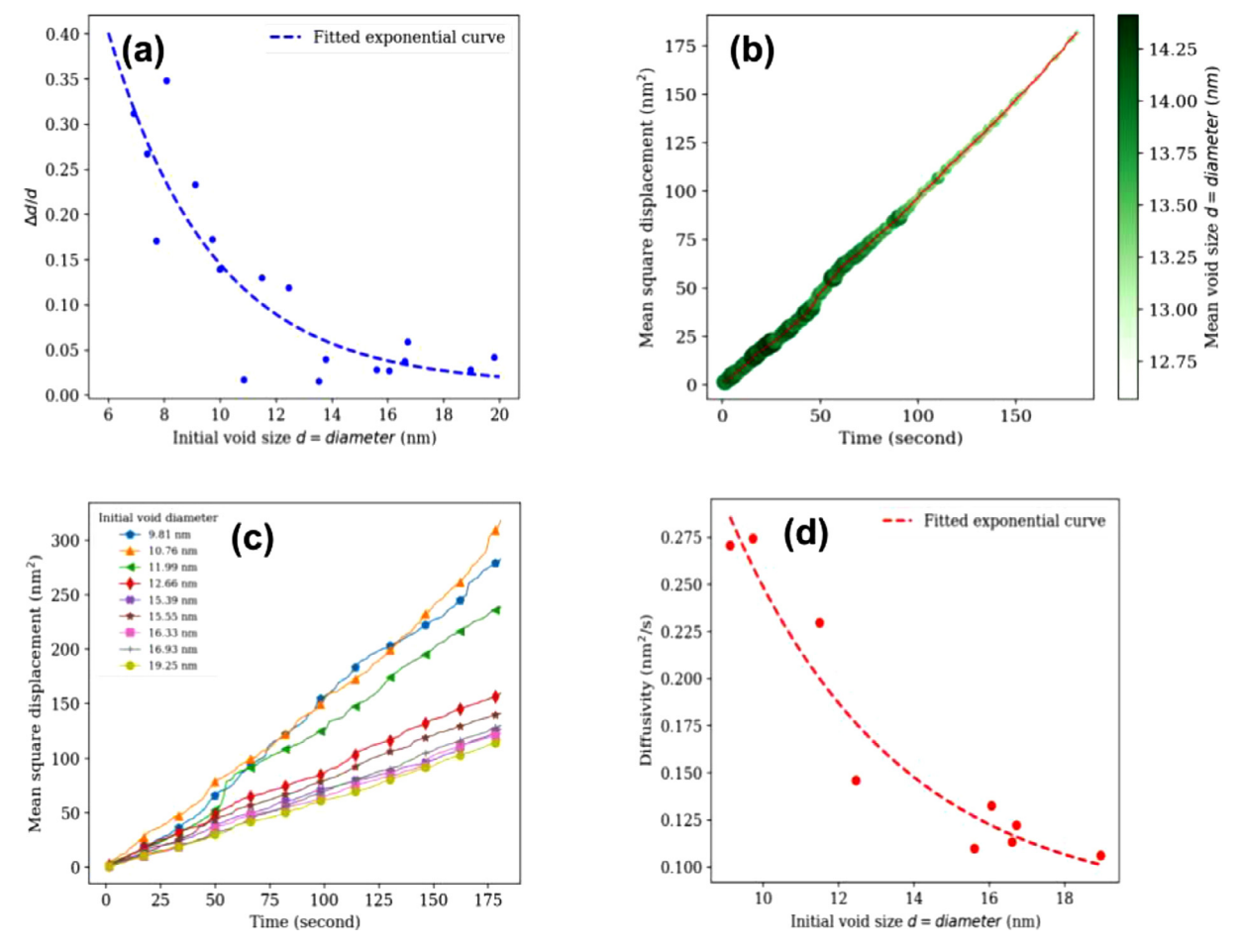


Fig. 4. (a) Normalized void diameter reduction ($\Delta d/d$) as a function of initial void size calculated using the data from U-Net model. Shrinkage is calculated as the percentage change of void diameter with respect to initial diameter. (b) Mean square displacement of 9 voids with different sizes (initial size diameter 9–18 nm). Note all data converge into nearly one straight line. Also, the thickness of the line indicates the average size of the voids at each timestep. The void sizes shrink with time as indicated by the decreasing thickness of the line. Here we used the average of 9 voids data for both size and mean square displacement. (c) Mean square displacements for each of the 9 voids plotted separately. We also show the best fit straight line for each of these 9 voids and find that smaller voids have higher slopes ($\overline{r^2}/t$), and hence higher diffusivity compared to larger voids (see supplementary Fig. S5). (d) Diffusivity of voids as function of initial void diameter. We used a 180 s in situ experiment video clip for all plots

terstitials and vacancies are introduced through the displacement-cascade event; however, there would not be a shrinkage in the long-time void evolution. In contrast, as the vacancy count in the core is reduced, the void size fluctuations would decrease, and the shrinkage of the void becomes more continuous. Moreover, the orientation-dependent gradient coefficient in the phase-field governing equation ensures anisotropy in the voids' surface energy.

Fig. 5(a–e) illustrate the configuration of cascades around the void in the simulations. In Fig. 5f, we compare the temporal evolution of two voids with different radius, 6 vs 12 (R6 vs R12). In general, both voids shrink over time; and the amplitudes of void size fluctuations are large for R6 compared to R12. A Gaussian kernel density estimate of the distribution of amplitude fluctuations for the two voids, shown in Fig. 5(g), indicates that the small void tends to have more frequent large size fluctuations than the bigger void. This plot is in qualitative agreement with Fig. 2b derived from machine learning data analyses. Such an observation from phase–field simulation is consistent with the measurements using the machine–learning tool on the experimental data.

To explain the fluctuations in void size, one must note the structure of the cascade assumed after the radiation event. After the four stages of the radiation event, the point defects form clusters at distinct locations of the cascade: vacancies occupy the inner core, while interstitials settle at the outer periphery. Moreover,

interstitials migrate much faster than vacancies because of their lower migration energy. As a result, the voids interact with waves of homogeneous point defect fluxes comprising either vacancies or interstitials. The voids would first interact with a wave of interstitials (due to their high mobility) followed by interaction with a secondary wave of vacancies. This series of alternating interactions of waves of point defects would result in the fluctuations of void sizes.

Next, we endeavor to explain the differences in amplitudes of fluctuations among voids with different sizes. By keeping the cascade nucleation the same across the simulations (for small and large voids), i.e., the cascades nucleate in same time at the same location, we ensured that the same number of point defects interact with the voids. Since a larger number of interstitials than the vacancies, interact with the voids, we observed void shrinkage. The reduction in the void area (ΔA), expressed as $\Delta A = 2\pi r \Delta r$ (where Δr is the void radius change) should be the same for both simulations because an equal number of point defects interact with both voids. It is evident from the relation that for a given reduction in the area, change in radius of the void is inversely related to the size of the void. Therefore, small voids undergo more considerable size changes (fluctuations) and thus explaining the size-dependent void size fluctuations observed in experiments and simulations.

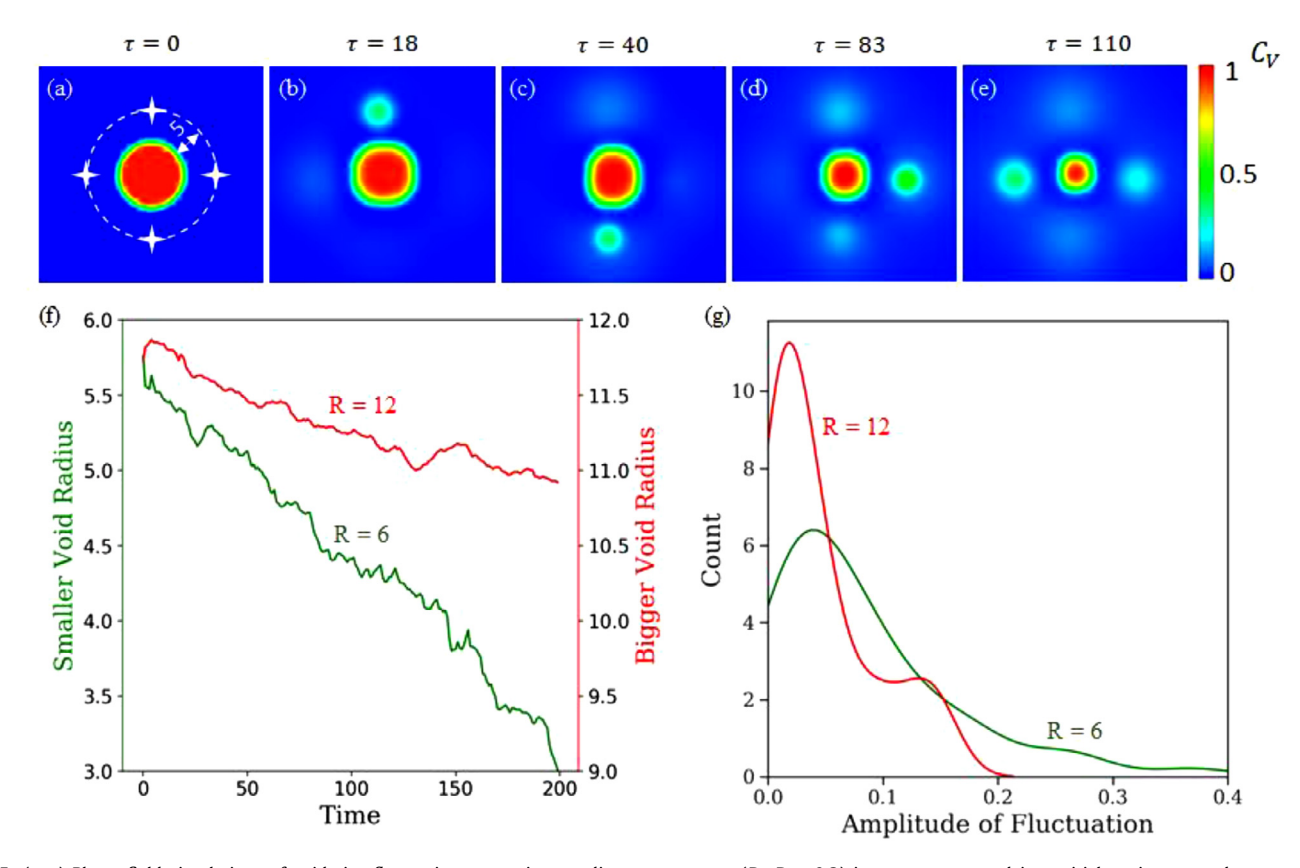


Fig. 5. (a–e) Phase–field simulations of void size fluctuations at an intermediate temperature $(D_v/D_i=0.2)$ in a supersaturated interstitial environment due to radiation cascades nearby, as illustrated in the snapshots. To investigate the fluctuation dependence on void size, two voids with different initial sizes (R = 6, 12) were considered. (f) The temporal evolution of the void sizes showing fluctuations. (g) Gaussian kernel density estimates of the distribution of amplitude of fluctuations for the two voids. Note the similarity between the simulation and experimental analysis in Fig. 2b.

In summary, we present the discovery of fluctuations in the nanovoid sizes during the *in situ* irradiation of Cu at an elevated temperature. This development was made possible through the automated measurement system, combining the convolutional neural network and the greedy tracking system. Manual measurements confirm that the void size fluctuations are indeed a physical phenomenon, not due to noise in neural network model output. Phase-field simulations also confirmed the size fluctuations, and we attributed them to the void interaction with alternating waves of point defect fluxes. Our method provides a general integrated framework to investigate other nanostructure evolutions in materials under extreme radiation environments.

Declaration of Competing Interest

The authors declare that they have no known competing financial interests or personal relationships that could have appeared to influence the work reported in this paper.

CRediT authorship contribution statement

M. Nasim: Conceptualization, Methodology, Investigation, Formal analysis, Writing – original draft. Sreekar Rayaprolu: Methodology, Validation, Formal analysis, Investigation, Writing – original draft. T. Niu: Methodology, Validation, Formal analysis, Investigation, Writing – original draft. C. Fan: Conceptualization, Methodology, Investigation, Formal analysis, Resources, Investigation, Writing – review & editing. Z. Shang: Investigation. Jin Li: Investigation. H. Wang: Investigation, Funding acquisition. A. El-Azab: Con-

ceptualization, Methodology, Investigation, Formal analysis, Writing – review & editing, Supervision, Project administration, Funding acquisition. **Y. Xue:** Conceptualization, Methodology, Investigation, Formal analysis, Writing – review & editing, Supervision, Project administration, Funding acquisition. **X. Zhang:** Conceptualization, Methodology, Investigation, Formal analysis, Writing – review & editing, Supervision, Project administration, Funding acquisition.

Data availability

Data will be made available on request.

Acknowledgments

We acknowledge financial support by NSF-CMMI-MOM 1728419. YX acknowledges financial support by NSF-CISE-IIS-1850243 and NSF-CISE-CCF-1918327. H. Wang acknowledges the support from the U.S. Office of Naval Research (N00014–16–1–2778). Access to the Life Sciences Microscopy Center and Materials Science Microscopy Center at Purdue University are also acknowledged. Work at the IVEM-Tandem Facility, ANL was supported by the U.S. Department of Energy, Office of Nuclear Energy under DOE Idaho Operations Office Contract DE–AC07–051D14517 as part of a Nuclear Science User Facilities experiment.

Supplementary materials

Supplementary material associated with this article can be found, in the online version, at doi:10.1016/j.jnucmat.2022.154189.

References

- B.N. Singh, S.J. Zinkle, Defect accumulation in pure fcc metals in the transient regime: a review, J. Nucl. Mater. 206 (1993) 212–229, doi:10.1016/0022-3115(93)90125-I.
- [2] M. Victoria, N. Baluc, C. Bailat, Y. Dai, M.I. Luppo, R. Schaublin, B.N. Singh, The microstructure and associated tensile properties of irradiated fcc and bcc metals, J. Nucl. Mater. 276 (2000) 114–122, doi:10.1016/S0022-3115(99)00203-2.
- [3] S.J. Zinkle, R.L. Sindelar, Defect microstructures in neutron-irradiated copper and stainless steel, J. Nucl. Mater. 155–157 (1988) 1196–1200, doi:10.1016/ 0022-3115(88)90495-3.
- [4] S.J. Zinkle, 1.03 Radiation-induced effects on microstructure Prepared for the Oak Ridge National Laboratory under Contract No. DE-AC05-000R22725, in: R.J.M.B.T.-C.N.M. Konings (Ed.), Elsevier, Oxford, 2012: pp. 65–98. 10.1016/B978-0-08-056033-5.00003-3.
- [5] S. Ishino, A review of *in situ* observation of defect production with energetic heavy ions, J. Nucl. Mater. 251 (1997) 225–236, doi:10.1016/S0022-3115(97) 00247-X.
- [6] G.R. Odette, M.J. Alinger, B.D. Wirth, Recent Developments in Irradiation-Resistant Steels, Annu. Rev. Mater. Res. 38 (2008) 471–503, doi:10.1146/ annurey matsci 38 060407 130315
- [7] R.E. Stoller, G.R. Odette, B.D. Wirth, Primary damage formation in bcc iron, J. Nucl. Mater. 251 (1997) 49–60, doi:10.1016/S0022-3115(97)00256-0.
- [8] S.J. Zinkle, G.S. Was, Materials challenges in nuclear energy, Acta Mater. 61 (2013) 735–758, doi:10.1016/j.actamat.2012.11.004.
- [9] S.J. Zinkle, 1.03-Radiation-Induced effects on microstructure, Comprehensive Nuclear Materials. 1 (2012) 65–98.
- [10] L.K. Mansur, Theory and experimental background on dimensional changes in irradiated alloys, J. Nucl. Mater. 216 (1994) 97–123, doi:10.1016/0022-3115(94) 90009-4
- [11] M.B. Toloczko, F.A. Garner, C.R. Eiholzer, Irradiation creep and swelling of the US fusion heats of HT9 and 9Cr-1Mo to 208 dpa at $\sim400^\circ\text{C}$, J. Nucl. Mater. 212–215 (1994) 604–607, doi:10.1016/0022-3115(94)90131-7.
- [12] H. Trinkaus, On the modeling of the high-temperature embrittlement of metals containing helium, J. Nucl. Mater. 118 (1983) 39–49, doi:10.1016/0022-3115(83) 90177-0.
- [13] S.J. Zinkle, K. Farrell, Void swelling and defect cluster formation in reactor-irradiated copper, J. Nucl. Mater. 168 (1989) 262–267, doi:10.1016/ 0022-3115(89)90591-6.
- [14] B.N. Singh, A. Horsewell, D.S. Gelles, F.A. Garner, Void swelling in copper and copper alloys irradiated with fission neutrons, J. Nucl. Mater. 191–194 (1992) 1172–1176, doi:10.1016/0022-3115(92)90659-9.
- [15] J.K. Steele, D.I. Potter, The disappearance of voids during 180 keV Ni+ bom-bardment of nickel, J. Nucl. Mater. 218 (1995) 95–107.
- [16] V.I. Dubinko, A.G. Guglya, E. Melnichenko, R. Vasilenko, Radiation-induced reduction in the void swelling, J. Nucl. Mater. 385 (2009) 228–230.
- [17] V.I. Dubinko, A.G. Guglya, S.E. Donnelly, Radiation-induced formation, annealing and ordering of voids in crystals: theory and experiment, Nucl. Instrum. Methods Phys. Res. B 269 (2011) 1634–1639, doi:10.1016/j.nimb.2010.12.012.
- [18] A.D. Marwick, Fluctuations in defect concentration due to inhomogeneous production of point-defects by collision cascades, J. Nucl. Mater. 116 (1983) 40–43.
- [19] V.I. Dubinko, V.F. Klepikov, The influence of non-equilibrium fluctuations on radiation damage and recovery of metals under irradiation, J. Nucl. Mater. 362 (2007) 146–151.
- [20] H. Gurol, W.G. Wolfer, Investigation of cascade-induced point-defect fluctuations, J. Nucl. Mater. 117 (1983) 244–249.
- [21] E.A. Koptelov, A.A. Semenov, Effect of collision cascade induced fluctuations in point defect concentrations on the void growth kinetics, Radiat. Eff. Defects Solids 113 (1990) 195–200.
- [22] E.A. Koptelov, A.A. Semenov, Instability conditions for a spatially homogeneous void distribution in irradiated metals, Phys. Status Solidi A Appl. Res. 89 (1985) 117–122.
- [23] A.A. Semenov, C.H. Woo, Void nucleation at elevated temperatures under cascade-damage irradiation, Phys. Rev. B 66 (2002) 24118.
- [24] A.A. Semenov, C.H. Woo, Fluctuations of point-defect fluxes to sinks under cascade damage irradiation, J. Nucl. Mater. 233 (1996) 1045–1050.
- [25] A.A. Semenov, C.H. Woo, Void swelling and spatial heterogeneity in microstructure evolution in pure metals at very low irradiation doses, J. Nucl. Mater. 212 (1994) 310–314.
- [26] A.A. Semenov, C.H. Woo, Stochastic fluctuations and microstructural evolution during irradiation by neutrons and heavy ions, J. Nucl. Mater. 205 (1993) 74–83
- [27] Y. Chen, K.Y. Yu, Y. Liu, S. Shao, H. Wang, M.A. Kirk, J. Wang, X. Zhang, Damage-tolerant nanotwinned metals with nanovoids under radiation environments, Nat. Commun. 6 (2015) 7036, doi:10.1038/ncomms8036.
- [28] T. Niu, M. Nasim, R.G.S. Annadanam, C. Fan, J. Li, Z. Shang, Y. Xue, A. El-Azab, H. Wang, X. Zhang, Recent studies on void shrinkage in metallic materials subjected to in situ heavy ion irradiations, JOM 72 (2020) 4008–4016, doi:10.1007/s11837-020-04358-3.

- [29] C. Fan, A.R.G. Sreekar, Z. Shang, J. Li, M. Li, H. Wang, A. El-Azab, X. Zhang, Radiation induced nanovoid shrinkage in Cu at room temperature: an in situ study, Scr. Mater. 166 (2019) 112–116, doi:10.1016/j.scriptamat.2019.02.046.
- [30] G. Roberts, S.Y. Haile, R. Sainju, D.J. Edwards, B. Hutchinson, Y. Zhu, Deep learning for semantic segmentation of defects in advanced STEM images of steels, Sci. Rep. 9 (2019) 12744, doi:10.1038/s41598-019-49105-0.
- [31] O. Ronneberger, P. Fischer, T. Brox, U-net: Convolutional networks for biomedical image segmentation, in: Proceedings of the International Conference on Medical Image Computing and Computer-Assisted Intervention, Springer, 2015, pp. 234–241.
- [32] Y. Li, S. Hu, X. Sun, F. Gao, C.H. Henager, M. Khaleel, Phase-field modeling of void migration and growth kinetics in materials under irradiation and temperature field, J. Nucl. Mater. 407 (2010) 119–125, doi:10.1016/j.jnucmat.2010.09.
- [33] Y. Li, D. Ma, B. Wang, Influence of bulk free energy density on single void evolution based on the phase-field method, Comput. Mater. Sci. 163 (2019) 100– 107, doi:10.1016/j.commatsci.2019.03.014.
- [34] D.O. Kharchenko, V.O. Kharchenko, Y.M. Ovcharenko, O.B. Lysenko, I.A. Shuda, L. Wu, R. Pan, Phase field modelling voids nucleation and growth in binary systems, Condens. Matter Phys. 21 (2018) 1–21, doi:10.5488/CMP.21.13002.
- [35] A.A. Semenov, C.H. Woo, Void nucleation at elevated temperatures under cascade-damage irradiation, Phys. Rev. B 66 (2002) 024118, doi:10.1103/ PhysRevB.66.024118.
- [36] S. Rokkam, A. El-Azab, P. Millett, D. Wolf, Phase field modeling of void nucleation and growth in irradiated metals, Model. Simul. Mater. Sci. Eng. 17 (2009), doi:10.1088/0965-0393/17/6/064002.
- [37] Z.H. Xiao, A.A. Semenov, C.H. Woo, S.Q. Shi, Single void dynamics in phase field modeling, J. Nucl. Mater. (2013), doi:10.1016/j.jnucmat.2013.03.076.
- [38] Y. Li, S. Hu, X. Sun, F. Gao, C.H. Henager, M. Khaleel, Phase-field modeling of void evolution and swelling in materials under irradiation, Sci. China Phys. Mech. Astron. (2011), doi:10.1007/s11433-011-4316-y.
- [39] A.A. Semenov, C.H. Woo, Phase-field modeling of void formation and growth under irradiation, Acta Mater. (2012), doi:10.1016/j.actamat.2012.07.049.
- [40] N. Wang, S. Rokkam, T. Hochrainer, M. Pernice, A. El-Azab, Asymptotic and uncertainty analyses of a phase field model for void formation under irradiation, Comput. Mater. Sci. 89 (2014) 165–175, doi:10.1016/j.commatsci.2014.03.045.
- [41] A.A. Semenov, C.H. Woo, Interfacial energy in phase-field emulation of void nucleation and growth, J. Nucl. Mater. 411 (2011) 144–149, doi:10.1016/j. inucmat 2011.01.100
- [42] P.C. Millett, S. Rokkam, A. El-Azab, M. Tonks, D. Wolf, Void nucleation and growth in irradiated polycrystalline metals: a phase-field model, Model. Simul. Mater. Sci. Eng. 17 (2009), doi:10.1088/0965-0393/17/6/064003.
- [43] Y. Wang, J. Ding, Y. Chen, J. Zhao, Y. Wang, Three-dimensional phase field simulation of intragranular void formation and thermal conductivity in irradiated α -Fe, J. Mater. Sci. 53 (2018) 11002–11014, doi:10.1007/s10853-018-2376-3.
- [44] A. El-Azab, K. Ahmed, S. Rokkam, T. Hochrainer, Diffuse interface modeling of void growth in irradiated materials. Mathematical, thermodynamic and atomistic perspectives, Curr. Opin. Solid State Mater. Sci. 18 (2014) 90–98, doi:10.1016/j.cossms.2014.01.002.
- [45] K. Ahmed, A. El-Azab, An analysis of two classes of phase field models for void growth and coarsening in irradiated crystalline solids, Mater. Theory 2 (2018) 1–36
- [46] P.C. Millett, A. El-Azab, S. Rokkam, M. Tonks, D. Wolf, Phase-field simulation of irradiated metals, Comput. Mater. Sci. 50 (2011) 949–959, doi:10.1016/j. commatsci.2010.10.034.
- [47] D. Schwen, S. Schunert, A. Jokisaari, Evolution of microstructures in radiation fields using a coupled binary-collision Monte Carlo phase field approach, Comput. Mater. Sci. 192 (2021) 110321, doi:10.1016/j.commatsci.2021.110321.
- [48] J. Li, C. Fan, J. Ding, S. Xue, Y. Chen, Q. Li, H. Wang, X. Zhang, *In situ* heavy ion irradiation studies of nanopore shrinkage and enhanced radiation tolerance of nanoporous Au, Sci. Rep. 7 (2017) 39484, doi:10.1038/srep39484.
- [49] C. Sun, D. Bufford, Y. Chen, M.A. Kirk, Y.Q. Wang, M. Li, H. Wang, S.A. Maloy, X. Zhang, *In situ* study of defect migration kinetics in nanoporous Ag with enhanced radiation tolerance, Sci. Rep. 4 (2014) 3737, doi:10.1038/srep03737.
- [50] Cuncai Fan, Rayaprolu Goutham Sreekar Annadanam, Zhongxia Shang, Jin Li, Meimei Li, Haiyan Wang, Anter El-Azab, Zhang Xinghang, Irradiation induced void spheroidization, shrinkage and migration in Cu at elevated temperatures: An in situ study, Acta Materialia 201 (2020) 504–516.
- [51] J. Li, K.Y. Yu, Y. Chen, M. Song, H. Wang, M.A. Kirk, M. Li, X. Zhang, *In situ* study of defect migration kinetics and self-healing of twin boundaries in heavy ion irradiated nanotwinned metals, Nano Lett 15 (2015) 2922–2927, doi:10.1021/ p150.46777
- [52] Radhakrishna Achanta, Appu Shaji, Kevin Smith, Aurelien Lucchi, Pascal Fua, Süsstrunk Sabine, SLIC superpixels compared to state-of-the-art superpixel methods, IEEE transactions on pattern analysis and machine intelligence 34 (11) (2012) 2274–2282.